Sixth International Symposium on Turbulence and Shear Flow Phenomena
Seoul, Korea, 22-24 June 2009

DIRECT NUMERICAL SIMULATION OF FLOW SEPARATION BEHIND A ROUNDED LEADING EDGE: STUDY OF CURVATURE EFFECTS

Eric Lamballais
Laboratoire d'Etudes Aérodynamiques UMR 6609,
Université de Poitiers, CNRS
Téléport 2 - Bd. Marie et Pierre Curie B.P. 30179
86962 Futuroscope Chasseneuil Cedex, France
eric.lamballais@univ-poitiers.fr

Jorge Silvestrini
Faculdade de Engenharia,
Pontifícia Universidade Católica do Rio Grande do Sul
Av. Ipiranga 6681, 90619-900 Porto Alegre - RS, Brasil
jorgehs@pucrs.br

Sylvain Laizet
Institute for Mathematical Sciences and Department of Aeronautics,
Imperial College London
53 Princes Gate, Exhibition Road,
South Kensington Campus, London SW7 2PG, UK
s.laizet@imperial.ac.uk

ABSTRACT

The separation bubble formed over a 2D half-body is studied by direct numerical simulation. The aim of this work is to consider the physical influence of the shape of the body that can be viewed as a thick half-plate with a front edge more or less rounded. The present generic body geometry is defined with a unique parameter $\eta = R/H$ corresponding to the ratio of the curvature radius R of the front edge over the body height H. In this paper, 16 calculations are presented depending on (i) the value of η with $\eta = 0.125, 0.25, 0.5, 1$; (ii) the 2D/3D nature of the computation; (iii) the inflow perturbations used to mimic residual turbulence in the free stream velocity U_∞. Only one Reynolds number $Re = U_\infty D/\nu$ is used for every simulation, allowing us to focus on the curvature effects over the separation bubble dynamics. To have a wide view of these effects, almost one order of magnitude separates the highest curvature from the lowest one considered here. The value of the Reynolds number ($Re = 2000$) combined with the resolution demand of the front edge (close to a sharp corner for the highest curvature case) requires to simulate the flow using up to 876 million mesh nodes. The curvature effects are found to deeply influence the separation bubble dynamics, with a significant expansion of the separated region size. This expansion is driven by the separation angle rise combined with the reinforcement of turbulence levels as the curvature is increased. These trends are associated with a change of bubble sensitivity with respect to upstream/downstream perturbations that can be interpreted in terms of convective/absolute stability.

INTRODUCTION

In many practical situations, flow separation is triggered by a sharp edge. In the context of bluff body, the shape of the edges can be advantageously smoothed to improve the aerodynamic characteristics of the body while better controlling the production of noise or vibrations. Despite the practical knowledge of these types of influence (especially in the car industry), there is no clear understanding of the physical mechanisms involved in the change of the resulting flow separation depending on the shape of the edge. In this study, our goal is to focus on this type of effect by considering a generic configuration where the flow separates over a rounded edge. The change of dynamics will be analyzed through its influence on (i) the mean flow (separation bubble features); (ii) the production of turbulent kinetic energy; (iii) the receptivity with respect to inflow perturbations.

In a previous study [9], we already have considered by direct numerical simulation (DNS) the curvature effects through comparisons between 2D and 3D flow separations behind two different front edges more or less rounded. Because interesting behaviours have been observed for purely 2D bodies, our purpose in this work is to focus on this type of geometry by considering a wider range of rounded edges. Additionally, in order to reduce the role of viscous effects on the dynamics, a higher Reynolds number is considered while maintaining the DNS strategy. This improvement of our results in terms of realism has required to increase drastically the computational effort with the help of the new generation of supercomputers.

FLOW CONFIGURATION AND NUMERICAL METHOD

Here, we consider the flow over a semi-infinite 2D body presenting a single curved leading edge. The flow configuration is presented in figure 1. Only a half model is considered through the imposition of mirror conditions (i.e. free-slip) at $y = 0$. This assumption allows the reduction of the computational storage by a factor two while fixing by construction the location of the stagnation point at $(x, y) = (x_s, 0)$ with

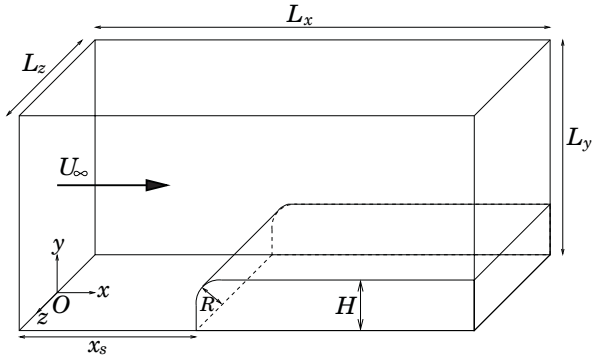

Figure 1: Schematic view of the flow configuration.

$x_s = 8H$. The present body geometry is fully determined by its height H and its constant edge radius R, with a unique nondimensional parameter $\eta = R/H$ with $0 \leq \eta \leq 1$. The value $\eta = 0$ refers to an infinitely sharp edge (squared corner) while $\eta = 1$ corresponds to a perfectly rounded leading edge over its full height (quarter round). Using the constant mean velocity U_∞ at the inflow section as reference velocity, the Reynolds number can be defined as $Re = U_\infty H/\nu$. The flow configuration in an infinite domain free from any perturbations is fully determined by the parameter couple η and Re. Here, four different curvatures are examined with $\eta = 0.125, 0.25, 0.5, 1$. To better identify the 3D effects, especially inside the separation bubble, these four flow geometries are compared using 3D and 2D DNS with ($u'_{\text{inflow}} \approx 0.1\%U_\infty$) and without ($u'_{\text{inflow}} = 0$) flow perturbations (16 calculations in total).

To simulate the flow, the DNS code "Incompact3d" is used in a recent version adapted to massively parallel supercomputers [8]. This code is based on compact sixth-order finite difference schemes for the spatial differentiation and a second order Adams-Bashforth scheme for the time integration [7]. The incompressible Navier-Stokes equations are directly solved in a computational domain $L_x \times L_y \times L_z = 20.25H \times 16H \times 6H$ on a Cartesian grid (stretched in y). The presence of the body is modelled with an immersed boundary method (IBM) adapted to the use of high-order schemes [10].

For the present study, an improvement of the method is carried out with the help of an extra-dissipation introduced artificially via the viscous term. This opportunity is offered by the use of compact schemes to compute second derivatives. This family of finite difference scheme can be easily adjusted to be over-dissipative on a narrow range of scales in the neighbourhood of the cutoff wave number associated with the grid. For a linear convection/diffusion equation, it can be shown that this extra-dissipation is more concentrated at the highest wave numbers (allowed by the grid) than the one introduced by high-order upwind schemes, even in a low-dissipation formulation like in [2]. We have observed that this numerical treatment, very easy to implement without any significant extra-computational cost (contrary to the use of an upwind formulation), is more effective and cheaper for the control of aliasing errors (non-negligible when high-order schemes are used) by comparison with a compact filtering of the non-linear terms for the present calculations. Moreover, the small wiggles created by the use of an IBM are also better reduced by the extra-dissipation compared with a filtering procedure. Here, only a local and explicit filtering of the non-linear terms is performed through a small patch located in front of the half-body. The use of this patch has been found to improve slightly the regularity of the solution in the near-body region without any detectable effects on the dynamics of the flow.

Two types of computational grid are used. For the moderate curvature cases $\eta = 0.25, 0.5, 1$, the use of $n_x \times n_y \times n_z = 1621 \times 451 \times 300$ mesh nodes allows us to reach $Re = 2000$ with a satisfactory numerical accuracy. Note that this spatial resolution ensures to describe the rounded edge geometry using at least 20 mesh nodes by curvature radius. To preserve this criterion, the case $\eta = 0.125$ has required to use a grid of $n_x \times n_y \times n_z = 3241 \times 901 \times 300$ mesh nodes while considering the same Reynolds number. For the 2D DNS ($n_z = 1$), exactly the same resolutions have been used. The boundary conditions imposed are inflow/outflow in x, free-slip in y and for 3D calculations, periodicity in z.

The inflow velocity U_∞ is perturbed by a low amplitude noise $u'_{\text{inflow}} \approx 0.1\%U_\infty$ computed to excite randomly and equally (in mean) all the length scales up to a cutoff wavelength of $H/6$. This noise is generated to admit a perfect time periodicity of $T = 40H/U_\infty$. Statistics are collected on a duration multiple of this particular time period (after a transient stage to obtain a well established flow) with an additional average in the homogeneous z-direction for 3D calculations. The marginal statistical convergence reached by 3D DNS using only a single period $T = 40H/U_\infty$ has been considered enough as far as the following analyses are concerned. Naturally, a quantitative study of low frequency phenomena would require to consider a clearly larger integration time to provide accurate statistics. For present 2D DNS, we have found that about ten time period (i.e. $400H/U_\infty$) is required to provide acceptable convergence due to the lack of average in z-direction.

RESULTS

As already mentioned, the present study is based on 16 calculations where 4 different front edge curvatures are considered by 2D and 3D DNS with and without inflow perturbations. All the data issued from these calculations have been exploited but in the rest of this paper, only a selection of results is presented to highlight the influence of η on the separation dynamics.

Instantaneous visualization

First, some comments should be made about results from 2D DNS. It is well known that the 2D assumption can lead to unrealistic flow, especially for the present separated flow that is highly unstable with respect to 3D perturbations. In consequence, present 2D DNS should be viewed as a reduced model where 3D motions are artificially prevented without expecting any relevancy with respect to the corresponding flow in real life. This point is illustrated in figure 2 where spanwise vorticity maps are compared from 2D and 3D DNS for the two extreme curvatures considered here, namely $\eta = 0.125, 1$. The resulting 2D dynamics is shown to differ drastically from the 3D ones, with a quasi-periodic vortex shedding from the bubble separation of very large structures. For these structures, clockwise vortices (of same vorticity as the shear layer at the start of the separation) dominate their counterclockwise counterparts formed in the near-wall region inside the separation. For the 3D results, a comparable formation of nearly-2D Kelvin-Helmholtz vortices can be recovered, but further downstream, the occurrence of a turbulence breakdown destroys the 2D coherence of the large

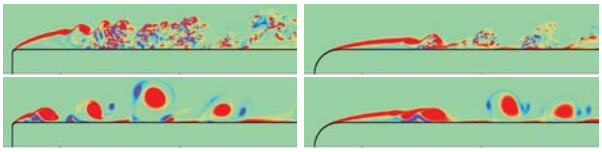

Figure 2: Maps of spanwise vorticity ω_z for $\eta = 0.125$ (left) and $\eta = 1$ (right) from 3D (top) and 2D (bottom) DNS with inflow perturbations.

scale structures as they travel through and behind the separation (see also figure 3).

A more complete view of the 3D dynamics can be obtained by volume visualizations of a characteristic vorticity isosurface as presented in figure 3 for the four curvatures considered. This type of view reveals clearly the highly 3D nature of the flow structures that develop in the separated region of the flow. Qualitatively, comparisons between the different body geometries show that the separation is deeply modified by the shape of the front edge with a more marked turbulent behaviour when the curvature is high. The breakdown to turbulence occurs clearly earlier as η is decreased through the appearance of small scale longitudinal vortices that fill the separated region. The resulting levels of vorticity are increased accordingly with a simultaneous scale reduction of the vortical structures, leading to the feeling that the Reynolds number is higher as η is decreased. Schematically, the observation of present visualizations suggests that the reduction of η increases the turbulence activity inside the separation bubble through physical mechanisms involving the direct excitation of the separated shear-layer. This point will be addressed in the following.

Bubble separation features

The examination of the mean flow allows the straightforward differentiation of the separation bubble obtained in each case. Here, we focus on the bubble size measured through its longitudinal and vertical expansion given by its reattachment length l_r and height h_r respectively. Note that l_r is estimated as $x_r - x_0$ where x_r is the streamwise location where the mean flow reattaches (detected here via the sign change of the longitudinal mean velocity at the first mesh node above the wall) while x_0 designates the end location of the body curvature ($x_0 = x_s + R$) where the separation is nearly observed for all the cases considered here. The resulting mean flow patterns are presented in figure 4 where some selected streamlines are plotted to highlight the separation bubble shape. Only cases with inflow perturbations are presented, the bubble separation structure being qualitatively similar without inlet excitation (for quantitative information, see table 1). As it can be expected, the changes between 2D and 3D dynamics leads to different mean flow as revealed by the important modifications of the separation bubble shape.

In terms of curvature effects, the reduction of η is found to reduce significantly l_r in 2D (up to -23%) while the opposite trend is observed in 3D (up to +40%) when inflow perturbations are imposed (see table 1). The 2D/3D differences of the bubble shape are less pronounced in its upstream part with virtually no modification of the separation angle θ (defined here as the direction of the mean flow at $x = x_0$ with respect to the horizontal direction). This suggests that the separation start remains purely 2D with a minor influence of downstream perturbations. The major influence of the separation angle is due to the body geometry where θ

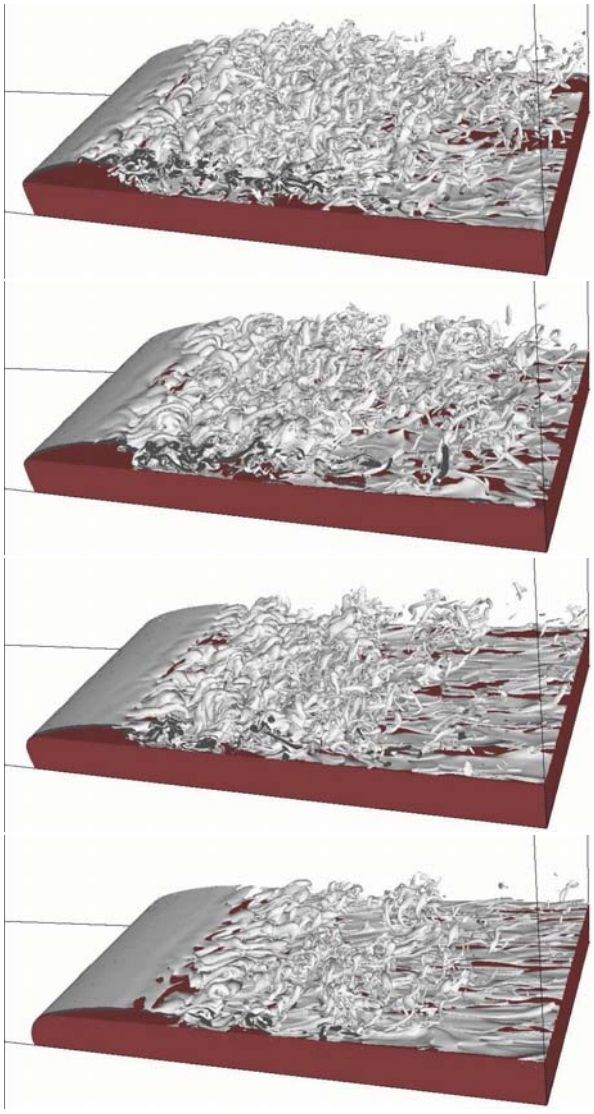

Figure 3: Perpective views of vorticity modulus isosurface $\omega = 8\,U_\infty^2/H$ for $\eta = 0.125, 0.25, 0.5, 1$ (from top to bottom). Results from 3D DNS with inflow perturbations.

goes from 15° at low curvature ($\eta = 1$) to 40° at the highest curvature ($\eta = 0.125$). This change of the separation orientation leads to an increase of h_r when the curvature is increased (see table 1). For a steady flow, it can be expected that a θ increase leads also to a l_r increase. However, for an unsteady separation, high turbulence levels are known to reduce the recirculation zone. Because the reduction of the curvature radius is found here to increase the turbulence levels, two antagonist effects can be expected. The combination of these two opposite influences leads to a reduction of l_r in 2D through the very high velocity fluctuations induced by the large scale vortices that control directly the reattachment. For the more realistic 3D dynamics, the turbulence breakdown limits the impact of velocity fluctuations so that the behaviour found corresponds more to the steady case, namely a l_r increase when θ is high (i.e. for high curvature).

Present l_r value for $\eta = 1$ is in good agreement with the one obtained by [12] in their LES ($l_r = 5.2H$ at $Re = 1725$) with a slight underestimation of 10% here. For $\eta = 0.125$, a more significant underestimation of about 25% is found in this work by comparison with the typical value $l_r = 10H$

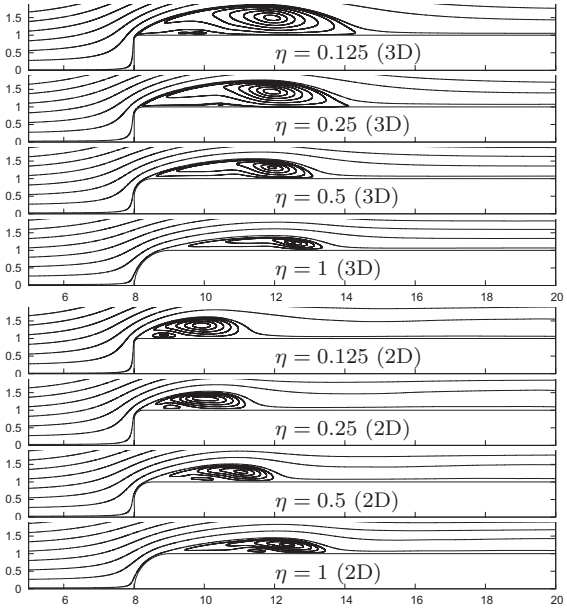

Figure 4: Mean streamlines for $\eta = 0.125, 0.25, 0.5, 1$. Results from 3D and 2D DNS with inflow perturbations.

Table 1: Recirculation length l_r, separation bubble height h_r, distance between the separation bubble centre and the separation point $\Delta x_c = x_c - x_0$, separation angle θ, maximum of the turbulent kinetic energy $k_{\max}$, minimal streamwise position $x_{\min}$ where $k > 1\%$, minimum value of the mean longitudinal velocity $U_{\min}$ (highest backflow intensity). Present results are normalized by H and U_∞. Values obtained with (left) and without (right) inflow perturbations.

	η	0.125	0.25	0.50	1
3D	l_r	6.6|7.8	5.9|7.4	4.8|6.8	4.7|7.0
	h_r	.88|.98	.77|.91	.57|.73	.42|.58
	$\frac{\Delta x_c}{l_r}$	.57|.58	.63|.66	.71|.75	.74|.79
	θ	40°|40°	32°|32°	23°|23°	15°|16°
	$k_{\max}$	.16|.15	.16|.15	.14|.15	.10|.11
	$\Delta x_{\min}$	1.3|1.4	1.9|2.7	2.2|3.7	2.8|4.6
	$U_{\min}$	-.38|-.34	-.35|-.33	-.30|-.31	-.24|-.23
2D	l_r	3.6|3.4	3.3|3.4	3.8|3.9	4.7|6.1
	h_r	.62|.59	.54|.55	.51|.52	.46|.56
	$\frac{\Delta x_c}{l_r}$	.50|.47	.56|.53	.66|.62	.70|.69
	θ	39°|39°	31°|31°	22°|22°	15°|15°
	$k_{\max}$	.30|.31	.27|.26	.22|.21	.14|.16
	$\Delta x_{\min}$	.13|.07	.20|.18	.65|.58	2.0|2.7
	$U_{\min}$	-.46|-.45	-.40|-.39	-.38|-.36	-.30|-.30

reported in the literature at higher Reynolds number for a sharp edge (see for instance [6, 11, 1]). Due to the uncertainty associated with the marginal statistical convergence reached here, it is difficult to conclude about the reason of this disagreement that could be associated with a 2D behaviour of the primary instabilities introduced by the low Reynolds number or by the limited spanwise extension of the computational domain used here.

An interesting change in the structural features of the separation bubble is related to the relative location of its centre detected as the singular point (of zero velocity) corresponding to a focus that is neither divergent nor convergent

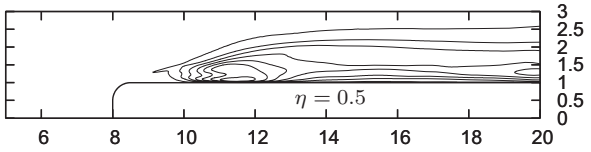

Figure 5: Turbulent kinetic energy k contours for $\eta = 0.5$ (contour levels from 0.01 by step of 0.03). Results from 2D DNS with inflow perturbations.

for the present 2D geometry [5, 9]. The examination of figure 4 clearly shows that the centre moves toward the reattachment point as the curvature is decreased, for 3D as well as for 2D results. This information is confirmed quantitatively in the table 1 where the different values of the distance $\Delta x_c = x_c - x_0$ between the centre streamwise location x_c and the separation point is reported for each case with a renormalization by l_r. This trend can be interpreted as a consequence of the instability source that moves toward the reattachment zone at low curvature with the creation of an extended "dead flow" region in the upstream part of the separation bubble where the flow is virtually stationary. In contrary, when the curvature is increased, the upstream shifting of the bubble centre leads to a reduction of this quiet zone, suggesting a corresponding displacement of the instability source. Note also the more complex structure of the separation bubble at $\eta = 0.125, 0.25$ where a secondary recirculation is unambiguously detected in 3D at a location where non-negligible perturbations can be suspected. This secondary bubble is always recovered in 2D, confirming that the bubble 2D dynamics responds to different excitation mechanisms compared with 3D cases.

Turbulent kinetic energy

To have a better idea about the location of the main unsteady regions of the flow, turbulent kinetic energy contours are presented in figure 6 for 3D cases with inflow perturbations. Qualitatively, similar pattern are obtained from 3D DNS without inflow perturbations with simply a shifting of the contours further downstream for the low curvatures cases (see next section). The corresponding 2D cases exhibit very different contours with a drastic increase of the turbulence levels and a different downstream evolution due to the unrealistic large-scale vortices for which the dissipation is negligible compared with the one associated with the 3D dynamics (see an example in figure 5). The main values associated with the turbulent kinetic energy k obtained in 2D regime are reported in table 1 without additional comments.

The more realistic 3D results exhibit (see figure 6) a rise of the turbulence levels as the curvature is increased, in agreement with the previous qualitative analysis based on instantaneous visualizations. The region for which k is significant is considerably enlarged for small η, with an increase of $k_{\max}$ up to 60% compared with the low curvature case $\eta = 1$. The location of $k_{\max}$ can be related with the separation bubble centre with a similar shifting toward the reattachment zone for low curvature cases. This moving of the turbulent production suggests again a change of the instability source locations driving the unsteady processes.

Additionally, it is worth noting that the streamwise location $x_{\min}$ of the more upstream significant non-zero k-contour (here, a threshold of 1% is chosen) moves toward the separation point as the curvature is increased. This behaviour is shown by table 1 where the distance $\Delta x_{\min} =$

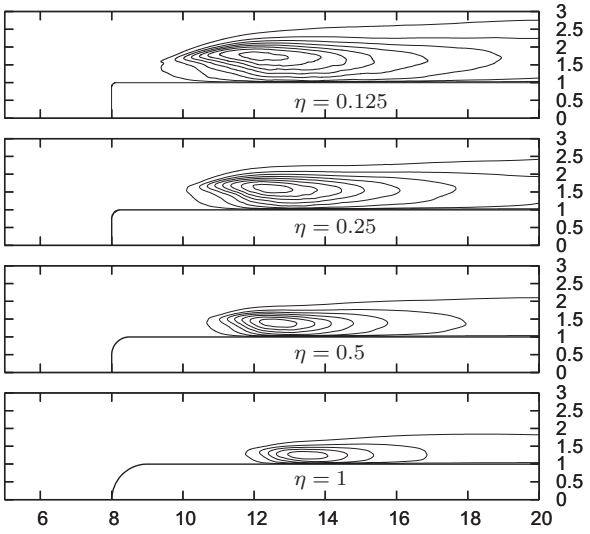

Figure 6: Turbulent kinetic energy k contours for $\eta = 0.125, 0.25, 0.5, 1$ (contour levels from 0.01 by step of 0.02). Results from 3D DNS with inflow perturbations.

$x_{\min} - x_0$ is reduced by more than 50% for the highest curvature case compared with $\eta = 1$. Note that the pike shaped of the lowest k-contour in its upstream part suggests that primary instabilities are triggered in the separated shear layer, this view being qualitatively confirmed by instantaneous visualizations. However, for $\eta = 0.125$, the upstream peak of the lowest k-contour is not exactly centred on the shear layer while being closer to the wall than for the other cases. This particular shape suggests a mechanism where turbulent perturbations are transported from downstream toward the separation point in the near-wall region by a reverse flow. This feature, directly connected to the receptivity of the flow with respect to inflow fluctuations, is the main subject of the two next sections.

Receptivity to inflow perturbations

In this section, we consider the influence of the inlet excitation through comparisons between the cases with and without inflow perturbations. First, it is useful to point out that the level of inlet excitation ($u'_{\text{inflow}} \approx 0.1\%U_\infty$) is low in order to correspond to a weak residual turbulence in the main stream. This is in contrast with our previous study [9] on laminar separation where the inflow fluctuations were 10 times higher in order to correspond to experiments in a water tunnel [4]. Here, the receptivity of the flow with respect to upstream fluctuations is discussed by comparison between results obtained with this slight upstream unsteady forcing and results free from any inflow perturbations except the unavoidable numerical errors of very low amplitude.

A strong sensitivity of the separation bubble with respect to the inlet perturbations can be noticed in table 1 at low curvature. For instance, l_r is found to increase by almost 50% in 3D (28% in 2D) for $\eta = 1$ when the inlet is free from perturbations, this strong effect being somewhat unexpected regarding the low level of inflow perturbations of the reference case. As the curvature of the front edge is more pronounced, this sensitivity of the bubble size is reduced with only a 18% increase of l_r at $\eta = 0.125$ when the inlet excitation is removed, a difference that is estimated within the uncertainty range associated with the statistical convergence reached in this study. For the 2D cases, a virtual removal of the inlet fluctuation influence can be observed from $\eta \leq 0.5$. This sensitivity of the flow with respect to inflow perturbations can be interpreted as a feature of convective instability while the receptivity reduction can be associated with an absolutely unstable behaviour. From this view, 2D mechanisms are found to increase the efficiency of absolutely unstable processes that seem to dominate the overall dynamics of the separation bubble. However, when 3D motions are allowed, the flow becomes unstable with respect to 3D perturbations, the resulting 3D dynamics being found more receptive to inflow fluctuations, especially for moderate curvature cases. To summarize, 2D mechanisms are found more efficient for the self-excitation of the flow but at the same time, they are dominated by 3D processes that decrease this efficiency while preserving the sensitivity of the flow with respect to inflow conditions, this sensitivity being gradually reduced as η is decreased.

An important observation is that with or without inflow excitation, all the flow considered here reach a self-sustaining unsteady state. This ability of the flow to be self-excited suggests the occurrence of absolutely unstable mechanisms governing the separation bubble dynamics. This is in contrast with our previous study [9] where the removal of inflow excitation was found to lead to a transient stabilization of the flow with a considerable enlargement of the separation bubble, its proximity with the computational domain exit having prevented us to pursuit the simulation. Here, this phenomenon is not recovered. This change of behaviour can be attributed to the use of a higher Reynolds number ($Re = 2000$ here against $Re = 1250$ in [9]) that seems to change the stability properties of the flow toward absolute instability mechanisms. This observation conciliates our previous and present results with the ones of [12] who have considered an intermediate Reynolds number ($Re = 1725$) with $\eta = 1$ while reporting that their flow was able to reach a self-sustaining state without significant influence of the inflow excitation.

Reverse flow inside the bubble

The intensity of the reverse flow inside the bubble can provide a preliminary idea about the more or less convectively unstable nature of present bubble separations. In table 1 are reported the highest backflow velocities $U_{\min}$ for each case. The velocity profiles at the corresponding x-locations are presented in figure 7 for the 2D and 3D results obtained with inflow perturbations. Note that very similar profiles are obtained for the cases without inflow perturbations, as suggested by the very close values of $U_{\min}$ reported in table 1 with and without inlet excitation. The major effect on $U_{\min}$ is due to the curvature that is found to increase gradually the backflow intensity (up to +50%) from $\eta = 1$ to $\eta = 0.125$ both in 2D and 3D. This behaviour is consistent with the previous comments suggesting the reinforcement of absolutely unstable mechanisms as the curvature is increased. This trend occurs in 3D as well in 2D, but the reverse flow is found to be stronger for the 2D cases and more concentrated in the near-wall region, consistently with the reduction of the bubble height h_r when 3D motions are prevented (see table 1).

A final remark about the backflow intensity can be made about the high values of $U_{\min}$ (in absolute value) even for the low curvature case in 3D. The minimal reverse flow is found to be 23% of U_∞, a higher value than the critical value of 15% obtained by [3] for the margin of convective/absolute stability in their bubble. Note that even a normalization using the maximum velocity at the same streamwise location

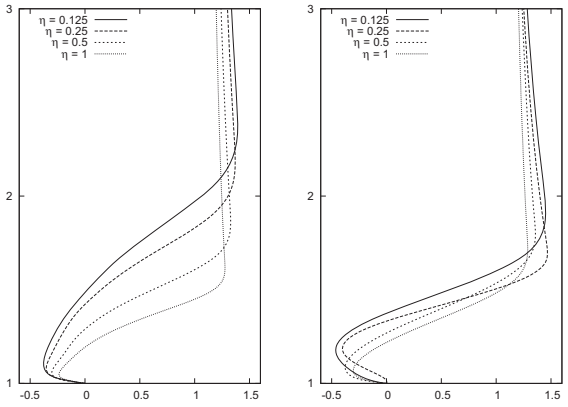

Figure 7: Comparison of mean longitudinal velocity profiles for $\eta = 0.125, 0.25, 0.5, 1$ at the streamwise location where the reverse flow is the strongest. Results from 3D (left) and 2D (right) DNS with inflow perturbations

as $U_{\min}$ leads to backflow always stronger than 18% for all the cases considered here. Despite the significant differences of present separation bubbles by comparison with [3], the present strong reverse flow suggests again the existence of an absolute instability region that governs the dynamics of every present separation bubble.

A last comment should be made about the disagreement between the present 23% reverse flow at $\eta = 1$ and the one less than 3% reported by [12] in their LES of a comparable flow. We have no explanation about this discrepancy.

CONCLUSION

The generic half-body considered here can be viewed as a thick half-plate with a front edge more or less rounded. In this study, we examine only the effect of the front-edge curvature by keeping constant the Reynolds number based of the half-body height H. For all the cases treated here, a separating-reattaching flow is obtained with a common feature of self-excitation in the separation bubble revealed by the ability of every flow to lead to self-sustaining unsteady processes without the need of any inlet excitation. Despite this common property, the basic change of the front-edge curvature is found to deeply influence the bubble dynamics.

These modifications can be observed directly on the mean flow through the enlargement of the bubble size controlled by antagonist effects associated with the increase of the separation angle combined with the turbulence reinforcement as the curvature is increased (i.e. η is decreased). Comparison between 2D and 3D DNS results shows that 3D motions dominate the bubble dynamics while decreasing the efficiency of self-excitation mechanisms, the artificial purely 2D dynamics being found to promote absolutely unstable processes. For the more realistic 3D DNS, a more marked absolutely unstable character is observed at high-curvature, with a clear reduction of the sensitivity of the flow with respect to inflow conditions.

To distinguish more precisely the upstream/downstream influences in the different flow regions, following the criterion proposed in a previous work on flow separation [9], a study of the deterministic response of the bubble dynamics with respect to the cyclic excitation is currently in progress. Additionally, to get quantitative information about the curvature influence in the absence of any turbulence fluctuations, we plane to compute the steady flow associated with each body geometry at the same Reynolds number. Such an artificial time truncation could be complementary to the present 3D truncation (offered by 2D DNS) to better distinguish the various mechanisms associated with the bubble transformation.

ACKNOWLEDGEMENTS

Present simulations have been performed using the supercomputers of GENCI at the IDRIS/CNRS and the CCRT. The authors are grateful to A. Spohn for his precious advices on this work.

REFERENCES

[1] I. E. Abdalla and Z. Yang. Numerical study of the instability mechanism in transitional separating-reattaching flow. *Int. J. Heat and Fluid Flow*, 25:593–605, 2004.

[2] N. A. Adams and K. Shariff. A high-resolution hybrid compact-ENO scheme for shock-turbulence interactions problems. *J. Comp. Phys.*, 127:27–51, 1996.

[3] M. Alam and N. D. Sandham. Direct numerical simulation of "short" laminar bubbles with turbulent reattachment. *J. Fluid Mech.*, 403:223–250, 2000.

[4] S. Courtine, A. Spohn, and J.-P. Bonnet. Vortex dynamics in the reattaching flow of separation bubbles with variable aspect ratio. In *Proc. of the 11th European Turbulence Conference, EUROMECH*, Porto, Portugal, 2007.

[5] J.-M. Delery. Robert Legendre and Henri Werlé: Toward the elucidation of three-dimensional separation. *Ann. Rev. Fluid Mech.*, 33:129–154, 2001.

[6] M. Kiya and K. Sasaki. Structure of large-scale vortices and unsteady reverse flow in the reattaching zone of a turbulent separation bubble. *J. Fluid Mech.*, 154:463–491, 1985.

[7] S. Laizet and E. Lamballais. High-order compact schemes for incompressible flows: a simple and efficient method with the quasi-spectral accuracy. *J. Comp. Phys.*, Submitted after revision, 2009.

[8] S. Laizet, E. Lamballais, and J. C. Vassilicos. A numerical strategy to combine high-order schemes, complex geometry and massively parallel computing for the DNS of fractal generated turbulence. *Computers and Fluids*, Submitted:1–27, 2008.

[9] E. Lamballais, J. Silvestrini, and S. Laizet. Direct numerical simulation of a separation bubble on a rounded finite-width leading edge. *Int. J. Heat and Fluid Flow*, 29(3):612–625, 2008.

[10] P. Parnaudeau, J. Carlier, D. Heitz, and E. Lamballais. Experimental and numerical studies of the flow over a circular cylinder at Reynolds number 3 900. *Phys. Fluids*, 20(085101), 2008.

[11] A. Suksangpanomrung, N. Djilali, and P. Moinat. Large-eddy simulation of separated flow over a bluff rectangular plate. *Int. J. Heat and Fluid Flow*, 21:655–663, 2000.

[12] Z. Yang and P. Voke. Large-eddy simulation of boundary-layer separation and transition at a change of surface curvature. *J. Fluid Mech.*, 439:305–333, 2001.